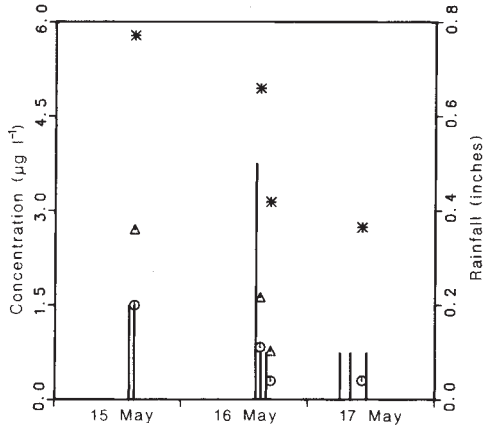

Fig. 3 Declining concentrations of alachlor (asterisks), metolachlor (triangles) and atrazine (circles) during a three-day rainy period at Tiffin, Ohio, 15-17 May 1985. Hourly rainfall is shown by the vertical lines.

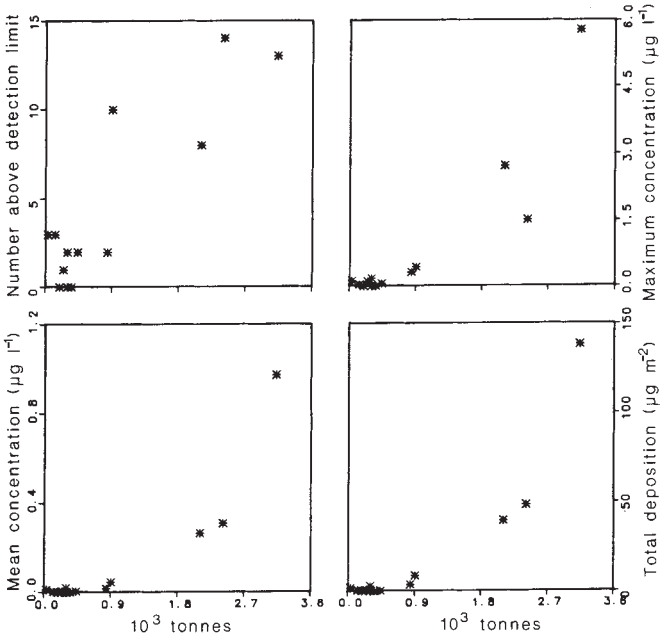

Fig. 4 Relationships between pesticide quantities used and measures of pesticide presence in rainfall. Values of r^2 range between 75% and 81%.

on most non-targeted plants are several orders of magnitude higher than concentrations observed in rainfall. Some aquatic algae and simple vascular plants show effects at or near these concentrations; however our data[4] indicate that impacts on these species are much more likely from surface runoff than from rainfall. The atmospheric residence time of moderately stable pollutants[15] indicates the possibility of widespread atmospheric dispersal of these compounds. Not enough is known about their pathways into and transport in the atmosphere, their temporal and spatial distribution patterns, and their partitioning in the atmosphere between vapor, water droplet solution, and sediment-adsorbed phases.

We thank Dr W. Moldenhauer, Dr David Helvey and Dr Thomas Young for collecting rainfall samples for us. This study was supported in part by the American Electric Power Service Corporation.

Received 16 September 1986; accepted 27 February 1987.

1. Hileman, B. *Envir. Sci. Technol.* **16**, 645A-650A (1982).
2. National Agricultural Chemicals Association *Report to the Membership for 1984-1985* (Washington, 1985).
3. Wauchope, R. D. *J. envir. Qual.* **7**, 459-472 (1978).
4. Baker, D. B. *J. Soil Water Conserv.* **40**, 125-132 (1985).
5. Baker, D. B., Krieger, K. A., Richards, R. P. & Kramer, J. W. in *Perspectives on Nonpoint Source Pollution* (ed. Moore, M. L.) 210-207 (Environmental Protection Agency, Washington, 1985).
6. Frank, R., Braun, H. E., Holdrinet, M. V. H., Sirons, G. J. & Ripley, B. D. *J. envir. Qual.* **11**, 497-505 (1982).
7. Johnson, H. P. & Baker, J. L. *Field-to-stream Transport of Agricultural Chemicals and Sediment in an Iowa Watershed: Part II. Data Base for Model Testing (1979-1980)* (Environmental Protection Agency, Athens, Georgia, 1984).
8. Hallberg, G. R., Libra, R. D. & Hoyer, B. E. in *Perspectives on Nonpoint Source Pollution* 109-114 (Environmental Protection Agency, Washington, 1985).
9. Soren, J. & Stelz, W. G. in *Perspectives on Nonpoint Source Pollution* 101-108 (Environmental Protection Agency, Washington, 1985).
10. Wu, T. L. *Wat. Air Soil Pollut.* **15**, 173-184 (1981).
11. Tabatabai, M. A. in *Agricultural Management and Water Quality* (ed. Schaller, F.) 92-108 (Iowa State University Press, 1983).
12. Bidleman, T. F. & Christensen, E. J. *J. geophys. Res.* **84**, 7857-7862 (1979).
13. Kramer, J. W. & Baker, D. B. in *Quality Assurance for Environmental Measurements, ASTM STP 867* (eds Taylor, J. K. & Stanley, T. W.) 116-132 (American Society for Testing and Materials, Philadelphia, 1985).
14. Waldron, A. C. *Ohio agric. Res. Dev. Cent. Bull.* **1157**, 1-12 (Ohio State University, 1984).
15. Glass, G. E. & Brydges, T. C. in *Acid Rain/Fisheries* (ed. Johnson, R. E.) 265-286 (NE Division of American Fisheries Society, Bethesda, 1982).

Small synoptic/mesoscale eddies and energetic variability of the eastern Levantine basin

Allan R. Robinson*, Artur Hecht†, Nadia Pinardi*, Jonah Bishop†, Wayne G. Leslie*, Zvi Rosentroub†, Arthur J. Mariano* & Steve Brenner†

* Center for Earth and Planetary Physics, Harvard University, Cambridge, Massachusetts 02138, USA
† Israel Oceanographic and Limnological Research, Ltd, Haifa, Israel

Mesoscale eddies are energetically dominant over most of the world's ocean[1]. The local dynamics of eddies is now a central problem of physical oceanography[2] and their statistics control aspects of the general circulation[3]. The horizontal scale of eddies is generally related to, but somewhat larger, than the Rossby internal deformation radius (the depth scale multiplied by the buoyancy frequency divided by the Coriolis frequency). In the eastern Mediterranean, which is not well explored or understood, the internal radius is known to be 12 km or 4 times smaller than in the North Atlantic. The study of such eddies requires very fine sampling which hinders their accidental discovery. By using a dedicated data set and objective analysis methods, we have established the existence of small synoptic/mesoscale eddies and jets, which constitute a variable and turbulent current regime and dominate the general circulation flow of the Levantine basin. Their existence in the Mediterranean has an impact on all aspects of basic and applied marine science there, both conceptually and with respect to experimental and monitoring programme designs.

The often cited general circulation data sets of Ovchinnikov and Fedorseyev[4] and Ovchinnikov[5] can reveal topographically controlled sub-basin-scale gyres, but do not hint at the mesoscale eddies. Even recent studies[6] depict the currents of the eastern Levantine basin as a smooth broad continuation of the North African current, following the coasts of the basin. South-east of Cyprus the current divides into two branches: one continuing northwards into the Cilician basin; the other turning westwards towards the centre of the Levantine basin. Thus, classically the circulation of the eastern Levantine basin consists of a large cyclonic gyre between Cyprus and the Egyptian coast with a smooth flow of the order of 5-10 cm s^{-1} between the surface and 500 m in all seasons.

A general circulation survey at 0.5° spacing in latitude and longitude[7] provided the motivation for carrying out a dedicated search for the small mesoscale eddies. We obtained and analysed a fine resolution data set in the southeastern Levantine basin during October 1985. The ~200 km^2 region south of Cyprus is presented in Fig. 1*a*; the topography consists of a small south-north gradient with a seamount located south-west of Cyprus. We now believe this to be the 'extension region' of the North

© 1987 Nature Publishing Group

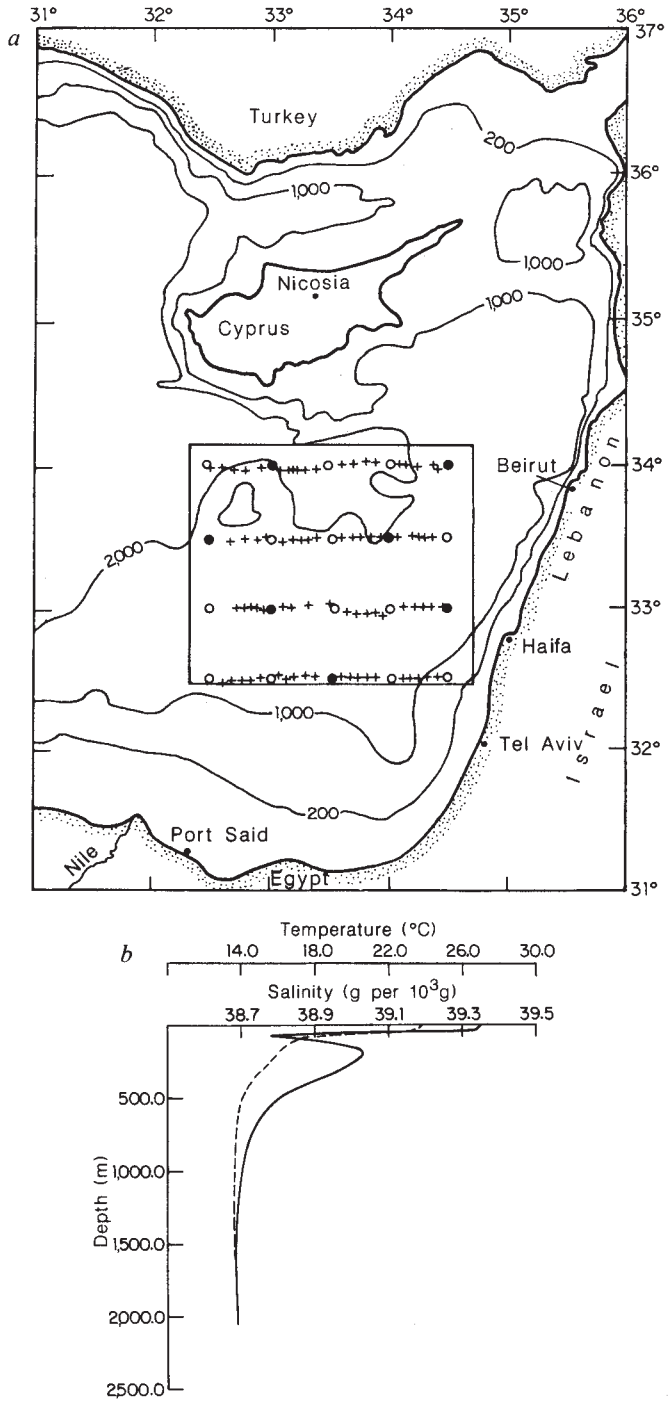

Fig. 1 *a*, The southeastern Levantine basin and bathymetric contours. The box indicates the domain of optimal interpolation. The circles show the CTD sampling scheme: open circles indicate casts down to about 1,000 dbar and full circles casts below 1,100 dbar. The crosses mark the positions of the XBT casts. *b*, The horizontally averaged temperature and salinity profiles for the combined XBT-CTD data set.

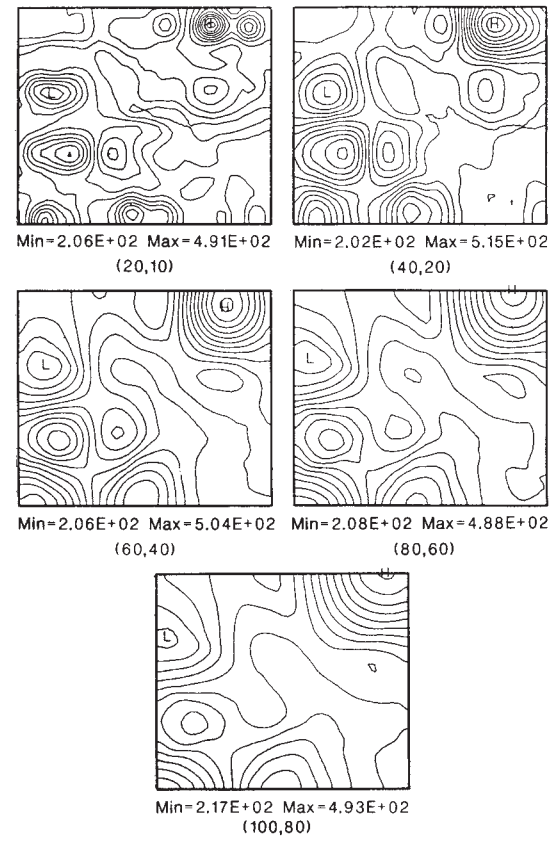

Fig. 2 Depth in metres of the 15 °C isotherm for the combined XBT-CTD data set. The numbers below each map indicate the value of the correlation length (decay length in km) assumed in the objective mapping correlation fucntion (see text). The contour interval is 20 m for each map. The numbers in parentheses denote the values of the parameters (*a*, *b*).

African current. The RV *Shikmona*, of the Israel Oceanographic and Limnological Research Institute, sampled this region with 82 expendable bathythermographs (XBTs) to 450 m at 10-km intervals (nominal) along the latitudinal tracks spaced 45 km apart and with twenty 1,100-m conductivity-temperature-depth (CTD) casts interspersed at 45-km intervals (every half degree of longitude) along the tracks. If a Rossby internal radius of deformation scaling were relevant, we would expect the diameter of the eddies to be about six times the internal radius. Thus, a sampling of the order of 10 km or less is expected to resolve the eddies along the track. The requirement of high resolution sampling along tracks which are relatively coarsely separated, for the definition of mesoscale features, has been discussed elsewhere[8].

We compared the XBT casts and the adjacent CTD temperature profiles; they agree within ±10 dbar in the first 50 m of the water column and are practically identical between 50 and 450 m. These results are consistent with previous investigations elsewhere[9,10]. The horizontally averaged temperature and salinity profiles from the combined CTD and XBT data sets are shown in Fig. 1*b*. The Levantine intermediate water layer, indicated by a subsurface salinity maximum, is found between 100 and 350 m with a relative salinity maximum at ~225 m. The temperature profile shows a very sharp temperature decrease in the first 100 m and a smaller main thermocline gradient down to 500 m. From comparison between repeated stations and examination of other data sets from the region, the high frequency internal wave noise on the temperature profiles is estimated to have an amplitude of the order of 5–10 dbar compared with the standard deviation of the mesoscale field presented here which is of the order of 50–60 dbar for the depth of the 15 °C isotherm.

A series of objectively analysed maps was made from the high-resolution combined CTD and XBT data sets. The domain is 220×180 km^2 and the grid spacing for the objective interpolation is 5 km. Since no previous mesoscale data sets exist, no statistics of the phenomena exist and therefore no *a priori* empirical correlation is available for objective analysis mapping[11]. Therefore, we chose a simple homogeneous, isotropic two parameter model, $C(r) = (1 - r^2/a^2) \exp(0.5\, r^2/b^2)$ with $r^2 = x^2 + y^2$ (ref. 12). To evaluate the parameters, (a, b), we

© 1987 Nature Publishing Group

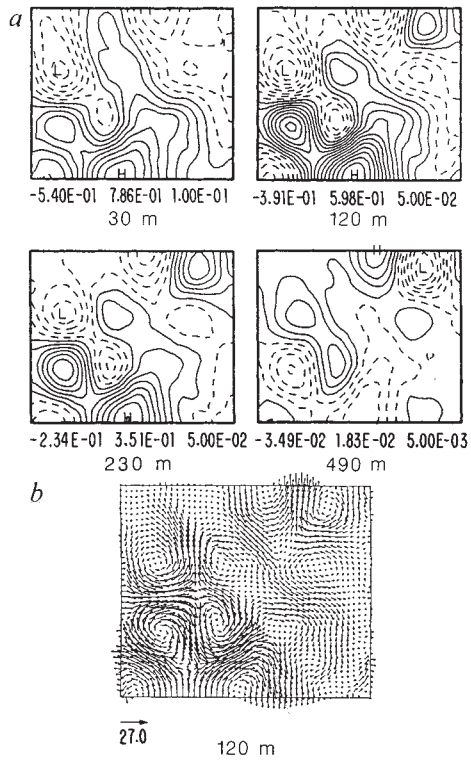

Fig. 3 *a*, Dynamic height anomaly at 30, 120, 230 and 490 m of depth: the horizontal average of the dynamic height at each level has been subtracted and the units are in $m^2 s^{-2}$. The values underneath each map represent the minimum, maximum and contour interval respectively. Solid contours indicate values above the horizontal average; broken contours indicate values below the horizontal average. The first solid contour equals the horizontal average. *b*, The geostrophic velocity structure at 120 m in units of cm s^{-1}. A reference arrow is shown at the left bottom corner.

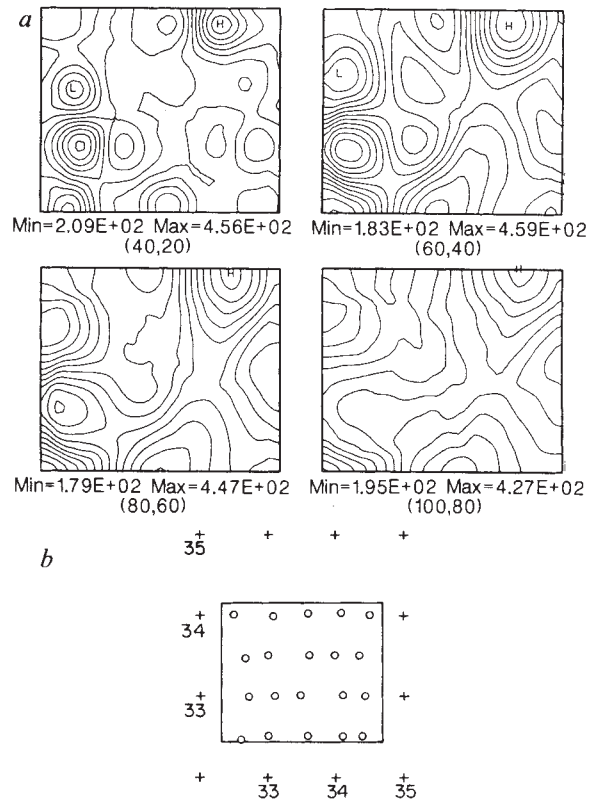

Fig. 4 *a*, Objective mapping of the depth of the 15 °C isotherm for a subsampled XBT data set. The numbers in parentheses below the maps indicate the correlation function parameters (see text) used for the mapping. The contour interval is 20 m for each map. *b*, The subsampled data coverage: 20 measurements are left from a total of 82 fine sampling XBT measurements. The crosses indicate a latitude, longitude grid where the numbers represent North latitude and East longitude. The open circles are the positions of the observations.

objectively map the same data with a range of parameter values and the compare these maps with each other and with those obtained by subjective mapping. The objective maps of the depth of the 15 °C isotherm of Fig. 2 show that the most reasonable and consistent results are obtained with the choice of $(a, b) = (40, 20)$ or $(60, 40)$. If the correlation parameters are larger then the interpolated field is over-smoothed. If the parameters are smaller, the maps contain the same eddies (except for a split north-east corner eddy) but they are smaller, sharper and separated by quiescent regions, which seems less realistic. The difference between the (40, 20) and (60, 40) experiments is in the strength of the eddy field, but until a correlation function is deduced from the data themselves the two cases are equivalent. We shall choose to use (60, 40) for further analysis and interpretation. For the parameters chosen each mapped eddy is defined by at least four observations.

The (60, 40) field of Fig. 2 is populated by small eddies ~60–70 km in diameter and by a somewhat larger-scale eddy feature (not fully contained in the domain) in the north-east. The local internal Rossby radius of deformation, calculated from the first eigenvalue of the linearized vertical quasi-geostrophic operator[13] using Fig. 1*b* profiles is 12.4 km. The small mesoscale field of Fig. 2 has a diameter 5–6 times the first internal Rossby deformation radius which is characteristic of such oceanographic phenomena generally. Maps of the temperature at several depths show the small eddies to have significant baroclinic amplitude at depths from 120 m to 330 m. Thus the small mesoscale eddy features have an intensified signature in the Levantine intermediate water layer.

In Fig. 3*a*, the dynamic height relative to 464 m is shown at several levels. This quite shallow reference level for the dynamic height has been chosen because it is the maximum depth common to all the XBT and CTD casts. The geopotential anomalies for XBT casts were computed from the XBT temperatures and the nearest CTD salinity. The dynamic height maps and the geostrophic velocity structure (Fig. 3*b*) show the intense small mesoscale eddies, embedded in a larger-scale flow composed of current filaments and jet segments. The North African current extension general circulation transport is probably contained in this flow but masked by the much stronger instantaneous mesoscale variability. The small mesoscale features have a strong vertically sheared structure with the baroclinic flow as intense as 20–30 cm s^{-1} in the upper thermocline levels. The near-surface 30-m geostrophic flow exhibits predominantly larger-scale structures.

The present data and analysis establish the existence of the eastern Mediterranean mesoscale but provide only one realization; the sampling requirements for future data sets are demanding. There does exist, however, in the region of Fig. 1*a* a several-year data set of >20 realizations obtained by the Israel Oceanographic and Limnological Research Institute scientists but with sampling essentially at the CTD locations only (the 'Marine Climate' or MC data). What, if any, information concerning mesoscale variability can be extracted from this data set? The sampling of 0.5° of latitude and longitude is regarded as 'fine general circulation sampling'; can it be regarded as 'coarse mesoscale resolution' sampling? To address this question we subsampled the October 1985 data set and intercompared maps of the subsampled data made with standard and coarse correlation functions. The results are shown in Fig. 4. We see that (40, 20) and (60, 40) maps do give a valid indication of the small mesoscale eddy field, although details differ from the best maps of Fig. 2 and only one or two data points define a feature.

© 1987 Nature Publishing Group

This is, however, encouraging because of the possibility of extracting at least qualitative synoptic and statistical mesoscale information from the MC data set which is uniquely extensive for the eastern Mediterranean. Preliminary results indicate highly variable eddies, jets and filaments with mesoscale variability exceeding seasonal variability.

We have searched for and identified the existence of mesoscale eddy variability in the southeastern Levantine basin. These eddies are of an absolute size about 4 times smaller than, for example, eddies in the North Atlantic, but bear the same approximate scale ratio to the local Rossby internal deformation radius. Their dynamics and role in the general circulation and in transport is not known, nor are the characteristics of mesoscale eddies elsewhere in the eastern Mediterranean. First evidence for the existence of mesoscale eddies in the western Mediterranean has also been recently documented with timescales from 5 to 30 days by Taupier-Letage and Millot[14]; the space scale is not well defined but thought to be small. The ratio between the relative vorticity and planetary vorticity advection is ~10 for the scales of motion involved[15]; thus geostrophic turbulence effects are expected to be more important than planetary wave propagation. Moreover, we suspect that nonlinear interactions between mesoscale eddies with important higher vertical mode coupling, to be potentially important in the Mediterranean. In particular, the southeastern Levantine small mesoscale eddies are Levantine-intermediate-water-intensified and could have an important role in transporting those water properties throughout the basin. The kinematic picture which is emerging, of strong eddies, jets and filaments dominating the flow and masking underlying mean current transports is consistent with results from other oceanic regions, for example, the north-east Atlantic[16] and the north-east Pacific[8].

Our research and the measurements from October 1985 were made in the context of the POEM (physical oceanography of the eastern Mediterranean) Program, which is a cooperative investigation of the eastern Mediterranean involving general circulation and mesoscale studies of theoretical and experimental nature[7] and which should provide a future context for determining the origin and role of the eddies. We thank the Intergovernmental Oceanographic Commission and Unesco Marine Science Program for helping to provide the POEM Scientific forums. We acknowledge the support of the Israel Oceanographic Limnological Research Institute and the NSF under a grant to Harvard University.

Received 27 October 1986; accepted 26 February 1987.

1. Robinsoson, A. R. in *Eddies in Marine Science* (ed. Robinson, A. R.) 1-14 (Springer, Heidelberg, 1983).
2. Haidvogel, D. B. in *Eddies in Marine Science* (ed. Robinson, A. R.) 404-436 (Springer, Heidelberg, 1983).
3. Holland, W. R., Harrison, D. E. & Semtner, A. J. Jr in *Eddies in Marine Science* (ed. Robinson, A. R.) 379-401 (Springer, Heidelberg, 1983).
4. Ovchinnikov, I. M. & Fedorseyev, A. F. in *Basic Features of the Geological Structure* 185-201 (1965).
5. Ovchinnikov, I. M. *Oceanology* **6**, 49-59 (1966).
6. Lacombe, H. *News. coop. Invest. Mediter.* **7**, 5-25 (1975).
7. POEM Steering Committee *UNESCO Reports in Marine Science* No. 35 (Unesco, Paris, France, 1985).
8. Mooers, C. N. K. & Robinson, A. R. *Science* **223**, 51-53 (1984).
9. Flierl, G. R. & Robinson, A. R. *J. phys. Ocean.* **7**, 300-302 (1977).
10. Heinmiller, R. H. in *Eddies in Marine Science* (ed. Robinson, A. R.) 542-567 (Springer, Heidelberg, 1983).
11. Bretherton, F. P., Davis, R. E. & Fandry, C. B. *Deep Sea Res.* **23**, 559-582 (1976).
12. Carter, E. F. & Robinson, A. R. *J. atmos. ocean. Technol.* (in the press).
13. Pedlosky, J. *Geophysical Fluid Dynamics* (Springer, Heidelberg, 1979).
14. Taupier-Letage, I. & Millot, C. *Oceanologica Acta* (in the press).
15. Robinson, A. R., Feliks, Y. & Pinardi, N. in *Proc. Lerici Workshop*, Lerici, Italy 1984 (ed. Charnok, H.) (in preparation).
16. Le Groupe Tourbillon *Deep Sea Res.* **30**, 475-511 (1983).

Temporal changes in microseismicity and creep near Parkfield, California

C. M. Poley, A. G. Lindh, W. H. Bakun & S. S. Schulz

US Geological Survey, 345 Middlefield Road, MS 977, Menlo Park, California 94025, USA

The 25-km-long section of the San Andreas fault near Parkfield, California ruptured in similar magnitude-6 earthquakes in 1881, 1901, 1922, 1934 and 1966. On the basis of a number of lines of seismological evidence, a section of the San Andreas fault, now termed the Parkfield preparation zone, has been identified as the locus of the next Parkfield earthquake[1-3]. Here we describe coincident changes in surface creep rates and deep seismicity near the Parkfield preparation zone following the 2 May 1983 Coalinga earthquake, and suggest that both respond to the same stimuli. These changes were concentrated near the point of initiation of the magnitude-6 characteristic Parkfield earthquakes, lending credence to the hypothesis that this section of the San Andreas fault is characterized by a unique set of physical properties[4-6] which make it ideal for earthquake prediction studies and which may also be useful for identifying hypocentral regions in other areas.

Epicentres near the trace of the San Andreas fault (A-A′ in Fig. 1) conform to a relatively simple pattern. Earthquakes between points A and B in Fig. 2*a*, located north-west of the Parkfield preparation zone (PPZ, Fig. 1), occur primarily between depths of 4 and 7 km, and correspond to the section of the San Andreas fault that is creeping at about 23 mm per yr[7]. Earthquakes between B′ and A′ in Figs 1 and 2*a*, south-east of the PPZ, tend to be deeper; their distribution resembles that of the aftershocks observed after the last characteristic Parkfield earthquake in 1966[8]. We have divided the area within the PPZ

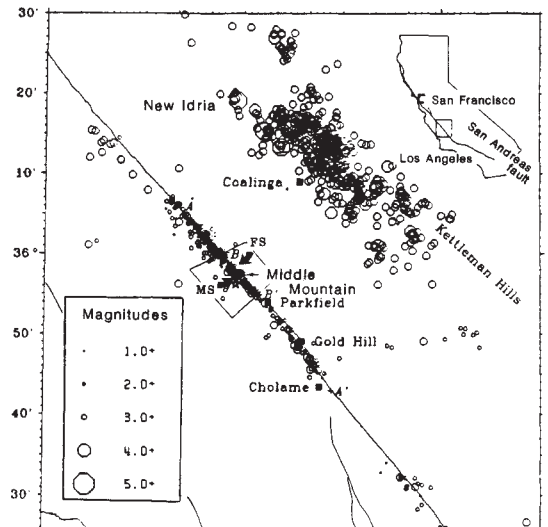

Fig. 1 Earthquake epicentres (1975-1985) relative to the trace of the San Andreas fault (long diagonal line) and the epicentres of the 1966 $M = 5.1$ foreshock and mainshock, shown as FS and MS respectively. Epicentre clusters east of the San Andreas fault are aftershocks of the 1975 Cantua Creek, 1976 Avenal, 1982 New Idria, 1983 Coalinga and 1985 Kettleman Hills earthquakes. Epicentres for all $M \geq 1.8$ earthquakes are shown, except the numerous $M \leq 3$ aftershocks of the 1983 Coalinga earthquake, which cover the Coalinga area when plotted. The Middle Mountain MM3 zone (quadrilateral) includes the preparation zone of the characteristic Parkfield earthquake.

© 1987 Nature Publishing Group